Indirect measurement of the 57.7 keV resonance strength for the astrophysical γ-ray source of the ^{25}Mg(p, γ)^{26}Al reaction

Y. J. Li (李云居)[1], Z. H. Li (李志宏)[1,2,*] E. T. Li (李二涛),[3] X. Y. Li (李鑫悦),[1] T. L. Ma (马田丽),[1]
Y. P. Shen (湛阳平),[1] J. C. Liu (刘建成),[1] L. Gan (甘林),[3] Y. Su (苏毅),[1] L. H. Qiao (乔律华),[1] Z. Y. Han (韩治宇),[1]
Y. Zhou (周勇),[1] J. Su (苏俊),[4] S. Q. Yan (颜胜权),[1] S. Zeng (曾晟),[1] Y. B. Wang (王友宝),[1] B. Guo (郭冰)[1]
G. Lian (连钢),[1] D. Nan (南丁),[1] X. X. Bai (白希祥),[1] and W. P. Liu (柳卫平)[1]

[1]*China Institute of Atomic Energy, P. O. Box 275(10), Beijing 102413, China*
[2]*School of Nuclear Science and Technology, University of Chinese Academy of Science, Beijing 101408, China*
[3]*College of Physics and Energy, Shenzhen University, Shenzhen 518060, China*
[4]*College of Nuclear Science and Technology, Beijing Normal University, Beijing 100875, China*

^{25}Mg(p, γ)^{26}Al is the most important reaction in the Mg-Al cycle in the hydrogen burning regions of stars. Its cross sections at stellar energies are essential to understand the issues of radioactive ^{26}Al in the galaxy and meteorites. The 57.7 keV resonance dominate the ^{25}Mg(p, γ)^{26}Al astrophysical reaction rates at relative low temperature, but it is very difficult to measure its resonance strength directly, and the indirect measurement results deviate by a factor of about 2 by far. In this work, the angular distributions of ^{25}Mg(^{7}Li, ^{6}He)^{26}Al leading to 6.364 MeV and eleven low-lying states in ^{26}Al have been measured by the Q3D magnetic spectrometer of the HI-13 tandem accelerator. The spectroscopic factors were derived and used to deduce the proton width and 57.7 keV resonance strength. The astrophysical ^{25}Mg(p, γ)^{26}Al reaction rates at stellar energies have been updated by using the present result.

I. INTRODUCTION

The origin of the long-lived radioactive nuclide ^{26}Al in the galaxy is a hot issue since the 1980s when the 1.809 MeV γ ray was detected [1,2] by the NASA's three High Energy Astronomy Observations (HEAO-3) spacecraft with cooled germanium detectors. Afterwards, observations were greatly improved by the Imaging Compton Telescope (COMPTEL) on board the Compton Gamma Ray Observatory (CGRO) and the International Gamma-Ray Astrophysics Laboratory (INTEGRAL) satellite. Subsequently, about 2.8 ± 0.8 M_{sun} total ^{26}Al mass were derived from the flux of 1.809 MeV γ ray [3] in our galaxy. The half-life of ^{26}Al is about 0.72 Myr, comparing with the multiple 10^9 of years age of the galaxy; this discovery provides a direct proof of the ongoing nucleosynthesis in our galaxy. Due to its slow decay, individual events cannot be detectable, observational results are from the cumulative yield of many events over the past 10^6 years. However, the discovery of ^{26}Al is the first detected γ-ray line emitted by radioactive nuclei in interstellar galactic gas, it established an important astronomical window of multimessenger studies.

Excesses of ^{26}Mg from the decay of ^{26}Al was also found in the Allende meteorite [4] and presolar dust grains [5]. The discoveries have two important meanings, one is that ^{26}Al is still alive at the time when the rocks were formed, it could

constrain the time interval between the latest nucleosynthesis event near the forming of our sun and give more information about the birth of our solar system, another one is that energy deposition from ^{26}Al decay injects a lot of heat, which could influence the forming of our earth.

However, there are some discrepancies between those observations and model calculations about ^{26}Al. First, the abundance of ^{26}Al in our early solar system is higher than the results detected by the γ-ray line of the present interstellar galactic gas. Second, the ratio of ^{26}Al/^{60}Fe in our early solar system is also higher than the observations [6]. Both of the discrepancies need more ^{26}Al to be produced in the early solar system. Therefore, it is important to study the ^{26}Al from both of model calculations and nuclear physics.

The ^{25}Mg(p, γ)^{26}Al astrophysical reaction rates are dominated by 57.7, 92.2, 190, 304 keV resonances. Many studies of the ^{25}Mg(p, γ)^{26}Al reaction have been carried out since 1970s [7–18], nevertheless, the direct measurements have only reached down to the 92.2 keV in the Laboratory of Underground Nuclear Astrophysics (LUNA) in 2012 [19,20]. Currently the 57.7 keV resonance can only be measured via indirect method due to the small yields and big background events in experiment. The ^{25}Mg(^{3}He, d)^{26}Al reaction leading to 6.364 MeV state have been performed at three different energies [7,13,14], and reanalyzed by Iliadis *et al.* to study 57.7 keV resonance, the derived proton spectroscopic factors agree with each other for the $l = 2$ components in measuring error ranges, while the $l = 0$ components deviate by about a factor of two, and the deduced resonant strength for 57.7 keV

_____
*zhhli@foxmail.com

resonance are also deviate almost by a factor of two [16]. Thus it is necessary to develop a new measurement to clarify this discrepancy.

The (^{7}Li, ^{6}He) single proton transfer reaction is suitable to measure the proton spectroscopic factors for the well-known ^{7}Li proton spectroscopic factor [21,22], and the shapes of the angular distributions can be well reproduced by the distorted wave Born approximation (DWBA) [23,24]. Therefore, the ^{25}Mg(^{7}Li, ^{6}He)^{26}Al reaction is chosen to solve this discrepancy.

In this work, the angular distributions of ^{7}Li elastic scattering on ^{25}Mg and ^{25}Mg(^{7}Li, ^{6}He)^{26}Al transfer reactions leading to 6.364 MeV and eleven low-lying states in ^{26}Al have been measured at $E(^7$Li$) = 31.5$ MeV. The ^{26}Al proton spectroscopic factors for the measured states were derived based on DWBA analysis by using the spectroscopic factor ratio calculated from shell model. The proton width and resonant strength of 57.7 keV resonance have been deduced, and then applied to calculate the astrophysical ^{25}Mg(p, γ)^{26}Al reaction rates at stellar energies.

II. MEASUREMENT

The experiment was carried out by using the Q3D magnetic spectrometer [25] with a 31.5 MeV ^{7}Li beam from the HI-13 tandem accelerator, Beijing. Similar to our previous experiments [26–28], the 200 enA ^{7}Li beam was impinged on a 75 μg/cm^2 thick ^{25}MgO target with a purity of 98.81%, which was sputtered on a 40 μg/cm^2 thick carbon foil. A ^{24}MgO target enriched to 99.85% in the same thickness was served as the background measurement. The thickness of the target was determined by an analytical balance with a precision of 1 μg. A removable Faraday cup at the down stream of the target was used to collect the beam for $\theta_{lab} > 6°$ normalization. A ΔE-E countertelescope was placed at 25° downstream of the target served as the relative normalization of measurements at angles of $\theta_{lab} \leqslant 6°$ to monitor the elastic scattering events. The reaction products were focused and determined by Q3D magnetic spectrometer with the accepted solid angle of 0.88 mSr for a good angular resolution, and measured by six X4 silicon detectors with each effective area of 75 mm × 40 mm on the focal plane. The X4 silicon detectors are composed of eight strips in the width of 5 mm with the 0.4 mm position resolution (FWHM) in length, and in sequence with the gaps of 55 mm on a high-precision motorized linear stages. In this layout, the obtained spectra of two measurements with the interval of 65 mm for the detector array position can be jointed to a continuous one with the length of about 800 mm, and the position distortion on the edge of the detectors can be eliminated effectively by the overlaps between two adjacent detecting areas.

The ^{25}Mg(^{7}Li, ^{6}He)^{26}Al* $_{6.364}$ reaction has been measured as the first aim in this experiment, the transfer reactions leading to ground and first ten excited states have been measured as well to deduce the direct capture component of ^{25}Mg(p, γ)^{26}Al and verify the spectroscopic factor proportions for different angular momentum components calculated from shell model. To extract the optical potential of the entrance channel, the ^{7}Li elastic scattering on ^{25}Mg

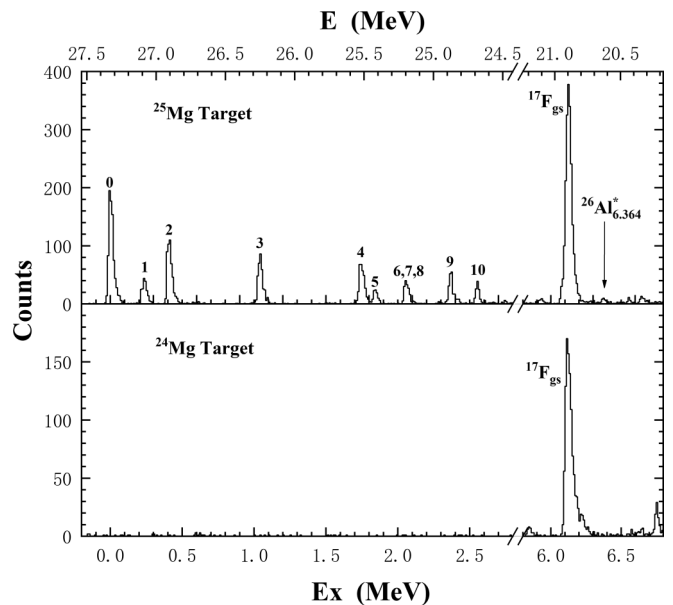FIG. 1. The spectra of the (^{7}Li, ^{6}He) reaction for ^{25}Mg and ^{24}Mg targets at $\theta_{lab} = 12°$, 0–10 represent the ground and first ten excited states in ^{26}Al.

has also been measured. The ratio of accumulated incident ^{7}Li ions on ^{25}Mg and ^{24}Mg targets is 2:1, and the typical spectra of the (^{7}Li, ^{6}He) reaction events for ^{25}Mg and ^{24}Mg targets at $\theta_{lab} = 12°$ are shown in Fig. 1. Each states in ^{26}Al can be found clearly in the spectra, and the ^{17}F events can be used to verify the position of 6.364 MeV state in ^{26}Al. The measured ^{25}Mg(^{7}Li, ^{7}Li)^{25}Mg elastic scattering angular distribution is shown in Fig. 2 and the angular distributions for the ^{25}Mg(^{7}Li, ^{6}He)^{26}Al transfer reactions are shown in Fig. 3.
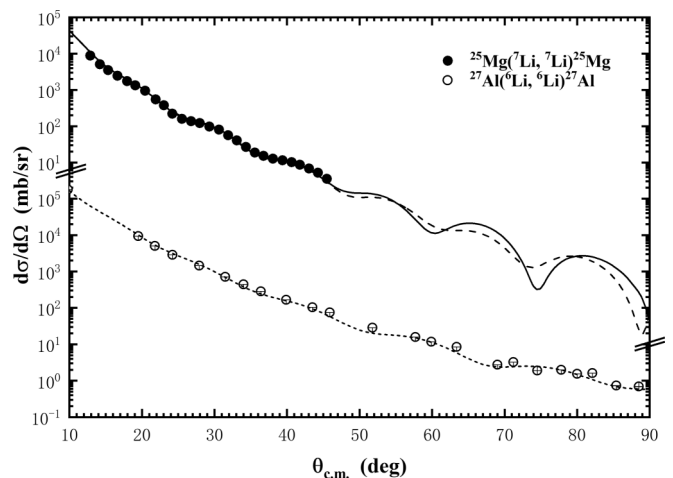
FIG. 2. Angular distributions for present ^{25}Mg(^{7}Li, ^{7}Li)^{25}Mg at $E(^7$Li$) = 31.5$ MeV and earlier ^{27}Al(^{6}Li, ^{6}Li)^{27}Al at $E(^6$Li$) =$ 18 MeV [29] are donated as solid and open circles together with the DWBA fitting results in different lines.

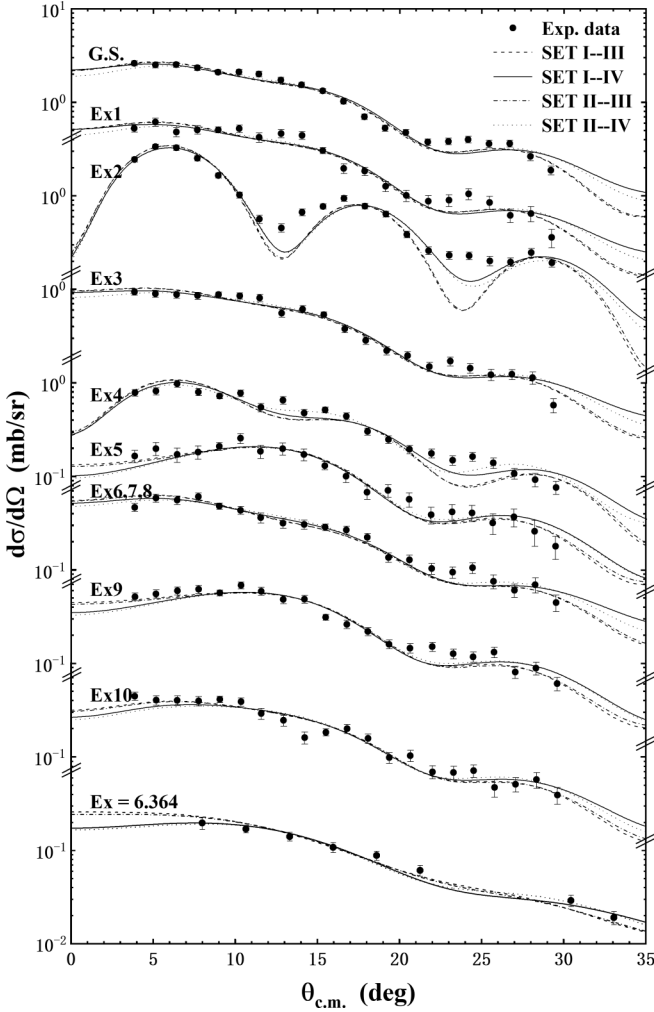FIG. 3. Measured angular distributions of ^{25}Mg(^{7}Li, ^{6}He) ^{26}Al transfer reactions together with the DWBA calculations in using the corresponding sets of optical potential parameters for the entrance and exit channels, respectively.

III. DWBA ANALYSIS

DWBA code FRESCO [30] was used to analyze the experimental angular distributions with the Woods-Saxon volume form factors for the potential [31],

$$U(r) = -\left[\frac{U_V}{1 + exp\left(\frac{r-R_R}{a_R}\right)} + \frac{iW_V}{1 + exp\left(\frac{r-R_I}{a_I}\right)} \right]. \quad (1)$$

U_V and W_V are the depths of the real and imaginary potentials, $R_i = r_i(A_p^{1/3} + A_t^{1/3})$, A_p, and A_t are the mass numbers of the projectile and target, r_i and a_i are the reduced radii and diffuseness of the potentials, and i can be either R or I for the real and imaginary parts of the potentials, respectively.

The Woods-Saxon optical potential parameters for the entrance channel were extracted from the ^{25}Mg(^{7}Li, ^{7}Li) ^{25}Mg angular distribution, which are listed in Table I as Sets I and II. No experimental data exist for the ^{6}He elastic scattering on ^{26}Al, then the potential derived by fitting the angular distributions of the ^{27}Al(^{6}Li, ^{6}Li) ^{27}Al at $E(^6$Li) = 18 MeV

TABLE I. Woods-Saxon potential parameters for the calculation of ^{25}Mg(^{7}Li, ^{6}He) ^{26}Al, Sets I, II, and III are extracted by fitting the ^{25}Mg(^{7}Li, ^{7}Li) ^{25}Mg and ^{27}Al(^{6}Li, ^{6}Li) ^{27}Al elastic scattering angular distributions, respectively. Sets IV and V are the global optical potentials for the exit channel ^{6}He + ^{26}Al and core-core ^{6}He + ^{25}Mg from Ref. [32], E is the corresponding laboratory energy of ^{6}He in MeV. The depths and geometrical parameters are in MeV and fm, respectively.

Set	U_V	r_R	a_R	W_V	r_I	a_I	r_C
I	85.6	0.799	0.845	10.4	1.260	0.831	1.0
II	233.0	0.612	0.850	16.5	1.140	0.880	1.0
III	162.0	0.878	0.832	11.6	1.372	0.487	1.2
IV	119.3 + 0.65E	0.9	0.7	8.1–0.15E	1.5	0.7	1.2
V	118.7 + 0.65E	0.9	0.7	8.0–0.15E	1.5	0.7	1.2

[29] and a ^{6}He global optical potential [32] were adopted for the exit channels and the parameters are listed in Table I as Sets III and IV, and the ^{6}He global optical potential also used for the core-core (^{6}He + ^{25}Mg) interaction in the calculations listed as Set V. As shown in Fig. 2, the angular distributions of elastic scattering were well fitted with their corresponding potential parameters.

For calculating the wave functions of the bound states, the Woods-Saxon potentials with the standard geometrical parameters $r_0 = 1.25$ fm and $a = 0.65$ fm were adopted, and the potential depths were adjusted automatically to reproduce the proton binding energies of the bound states in ^{26}Al. Then the transfer reactions have been calculated by using above optical potential parameters. Since the unbound state cannot be handled, the angular distributions of $J^\pi = 3^+$ states with the excitation energies for a bound state ranges from 6.0 to 6.3 MeV in an energy step of 50 keV have been calculated. As shown in Fig. 4, the shape of these angular distributions did not show noticeably change and the differential cross sections decreased linearly with the increase of excitation energy at forward angles. Then the differential cross sections of
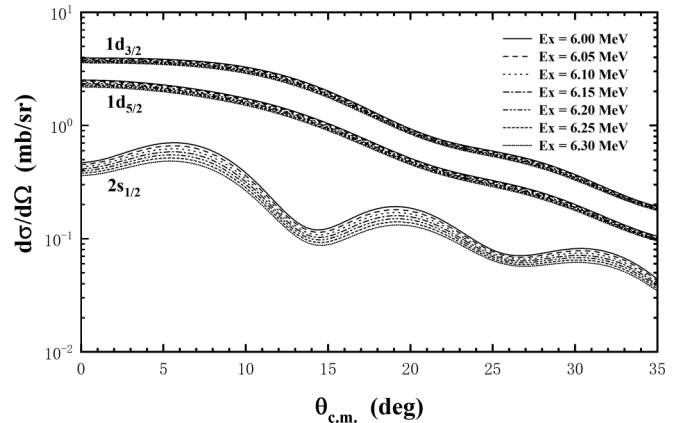

FIG. 4. Calculated angular distributions of ^{25}Mg(^{7}Li, ^{6}He) ^{26}Al leading to $J^\pi = 3^+$ states with the excitation energies range from 6.0 to 6.3 MeV in energy step of 50 keV.

TABLE II. Proton spectroscopic factors for the relevant states in ^{26}Al. E_x is the excited energy for each states, C^2S_{th} and C^2S_{exp} are the calculated and experimental spectroscopic factors for the $2s_{1/2}$, $1d_{3/2}$, and $1d_{5/2}$ orbits.

E_x (MeV)	J^π	C^2S_{th}			C^2S_{exp}		
		$2s_{1/2}$	$1d_{3/2}$	$1d_{5/2}$	$2s_{1/2}$	$1d_{3/2}$	$1d_{5/2}$
0.0	5^+			0.521			0.60 ± 0.07
0.2283	0^+			1.235			1.51 ± 0.17
0.4169	3^+	0.317	0.013	0.018	0.29 ± 0.04	0.012 ± 0.001	0.017 ± 0.002
1.0577	1^+		0.007	0.703		0.009 ± 0.001	0.86 ± 0.10
1.7590	2^+	0.139	0.190	0.018	0.15 ± 0.02	0.20 ± 0.03	0.019 ± 0.003
1.8506	1^+		0.121			0.17 ± 0.02	
2.0689	4^+			0.012			0.016 ± 0.002
2.0695	2^+	0.017	0.008	0.174	0.023 ± 0.003	0.011 ± 0.001	0.24 ± 0.03
2.0716	1^+			0.021			0.029 ± 0.004
2.3652	3^+		0.112	0.015		0.20 ± 0.02	0.026 ± 0.003
2.5454	3^+	0.016	0.085	0.066	0.015 ± 0.002	0.078 ± 0.009	0.061 ± 0.007
6.3640	3^+	0.071	0.140	0.024	0.082 ± 0.012	0.16 ± 0.02	0.028 ± 0.004

6.364 MeV state were extrapolated with the variation of excitation energies.

The ^{26}Al proton spectroscopic factor $C^2S_{26Al}^{l_p j_p}$ can be derived by normalizing the DWBA calculations to the experimental data according to the expression

$$\left(\frac{d\sigma}{d\Omega}\right)_{exp} = \sum_{l_p j_p} C^2 S_{^7Li} C^2 S_{26Al}^{l_p j_p} \left(\frac{d\sigma}{d\Omega}\right)_{DWBA}^{l_p j_p}, \qquad (2)$$

where $(d\sigma/d\Omega)_{exp}$ and $(d\sigma/d\Omega)_{DWBA}$ are the measured and calculated differential cross sections, respectively. The proton spectroscopic factor of ^{7}Li has been determined as 0.42 based on Refs. [21,22].

The proton spectroscopic factors of ^{26}Al were analyzed with the shell model code NUSHELL@MSU [33] by using usdbpn Hamiltonian [34] in the sdpn model space, and the calculated results for the $2s_{1/2}$, $1d_{3/2}$, and $1d_{5/2}$ orbits are listed in Table II. Then the ratios of the calculated spectroscopic factors for each component were adopted in the calculation of the transfer reactions, and the results are also shown in Fig. 3 together with the experimental data. One can see that the angular distributions of the ^{25}Mg(^{7}Li, ^{6}He)^{26}Al transfer reaction leading to 12 states in ^{26}Al are well reproduced with J^π from 0^+ to 5^+ and the varied proportion of $2s_{1/2}$, $1d_{3/2}$, and $1d_{5/2}$ components. Then the derived spectroscopic factors of each components for all the measured states are listed in Table II, the proton spectroscopic factors of the 6.364 MeV state in ^{26}Al are 0.082 ± 0.012, 0.162 ± 0.024, and 0.028 ± 0.004 for the $2s_{1/2}$, $1d_{3/2}$, and $1d_{5/2}$ orbits, respectively, the uncertainties are mainly come from the divergence of optical potential parameters (9%), the error of the measurement (5%) and ^{7}Li spectroscopic factor (10%) [21].

Angular distributions of the ^{25}Mg(^{3}He, d)^{26}Al$^*_{6.364}$ reaction at three energies [7,13,14] have also been reanalyzed as the above procedure. For the convenience of the calculations, the DWBA calculation code TWOFNR [35] have been adopted since the proton spectroscopic factor of ^{3}He has been embedded and one set of the optical potential parameters for the entrance channel from Ref. [36] and three sets for the exit channel from Refs. [36,37] were included in the

code. The calculations together with the experimental data are shown in Fig. 5, three (^{3}He, d) angular distributions are all well reproduced with the calculated spectroscopic factor proportions of $2s_{1/2}$, $1d_{3/2}$, and $1d_{5/2}$ components for 6.364 MeV state. The ratio of the experimental and calculated spectroscopic factors C^2S_{exp}/C^2S_{th} for the present (^{3}He, d) reanalysis is obtained to be 1.33 ± 0.20, it is in agreement with the present ^{25}Mg(^{7}Li, ^{6}He)^{26}Al$^*_{6.364}$ result 1.16 ± 0.17 within the uncertainty.

IV. REACTION RATES

The reaction rate for a narrow and isolated resonance is given by

$$N_A \langle \sigma v \rangle = \sum_i N_A \left(\frac{2\pi}{\mu kT}\right)^{3/2} \hbar^2 e^{-E_R^i/kT} f_i \omega \gamma_i, \qquad (3)$$
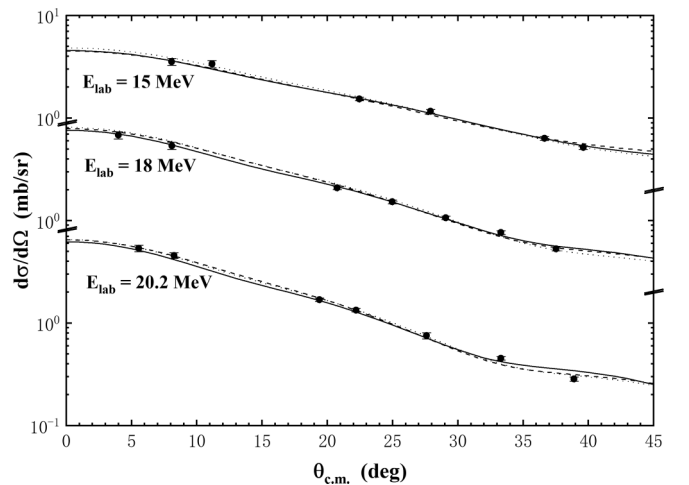

FIG. 5. Angular distributions of ^{25}Mg(^{3}He, d)^{26}Al$^*_{6.364}$ at three energies [7,13,14] together with corresponding DWBA calculations. Three types of the lines are the angular distributions calculated with one set of the optical potential parameters for the entrance channel and three sets for the exit channel included in TWOFNR code.

where N_A and k denote the Avogadro's and Boltzmann's constant, μ is the reduced mass, T is the stellar temperature, E_R^i is the resonant energy of the ith resonance, f_i is the ground-state feeding probability and the resonance strength $\omega\gamma_i$ for the (p, γ) reaction is expressed as:

$$\omega\gamma_i = \frac{(2J_i + 1)}{(2j_p + 1)(2j_t + 1)} \cdot \frac{\Gamma_p \Gamma_\gamma}{\Gamma_{tot}}, \qquad (4)$$

where J_i, j_p, and j_t are the spins of ith resonance, proton, and target, respectively. Γ, Γ_p, Γ_γ are the total energetic width, the proton partial energetic width and γ width, respectively.

Proton partial width Γ_p can be calculated based on the relation [38]

$$\Gamma_p = \sum_l 2 \frac{\hbar^2}{\mu a_c^2} C^2 S_l \cdot P_l \cdot \theta_{sp}^2, \qquad (5)$$

where the channel radius a_c is defined as $r_0(A_T^{1/3} + A_p^{1/3})$, in this place, A_T and A_p is the atomic mass number of ^{25}Mg and proton, $C^2 S_l$ is the proton spectroscopic factor and P_l is calculated penetration factor with the orbital angular momentum l, and the single-particle reduced width $\theta_{sp}^2 = a_c \phi_l^2(a_c)/2$ [39]. The θ_{sp}^2 also have been calculated with the excitation energies for a bound state ranges from 6.0 to 6.3 MeV in energy step of 50 keV, and its value vary only 0.4% and 3% for $l = 0$ and 2. Then the single-particle reduced widths of 6.364 MeV state were extrapolated with the variation of excitation energies.

For the 57.7 keV resonance, $P_0 = 3.33 \times 10^{-18}$ much bigger than $P_2 = 2.32 \times 10^{-20}$, therefore the proton partial width is dominated by $l = 0$ component and computed to be $(5.03 \pm 0.74) \times 10^{-13}$ eV based on the present $(^7\text{Li}, {}^6\text{He})$ result. The γ width is estimated to be 0.03 eV much bigger than the proton width, and the total width approximately equal to the gamma width, the resonance strength will only be relate to proton width according to Eq. (4). In addition, in order to study the influence of the bound-state form factor on the resonance strength, r_0 and a are varied in the ranges of 1.15–1.35 and 0.55–0.75, the divergences of the resonance strength are 3.7% and 8.4% for one σ confidence intervals, respectively. Then the resonance strength of 57.7 keV resonance is derived to be $(2.93 \pm 0.50) \times 10^{-13}$ eV.

To calculate the total reaction rates, our updated data for 57.7 keV resonance and the parameters adopted in Ref. [20] for the rest resonances have been used as shown in Table III. For the resonant strength derived from the direct measurement, electron screening effect enhancement factor f_{es} should be adopted as the approximation of $\exp(\pi\eta U_e/E_r)$ [45], where η is the Sommerfeld parameter and U_e is the screening potential with a value of 1.14 keV [46].

The uncertainty of $\pm 1\sigma$ confidence intervals have been determined via the Monte Carlo method by generating the Gaussian random of $\omega\gamma_i$ and f_{es} with the corresponding values and errors, where 30% of the difference between value and unity of electron screening factors was assigned as uncertainty to account for the theoretical ambiguity. The Gaussian randoms of feeding probability f_i have also been generated for calculating the reaction rates of the ground state, and $(1 - f_i)$ have been used for the isomeric state.

TABLE III. Parameters have been used in the present calculation of the ^{25}Mg(p, γ)^{26}Al reaction rates, and for the resonances not listed here were taken from Ref. [40].

E_R[a] (keV)	$\omega\gamma$ (eV)	f_0	f_{es}
37.0	$(4.5 \pm 1.8) \times 10^{-22}$[b]	0.79 ± 0.05[c]	
57.7	$(2.9 \pm 0.5) \times 10^{-13}$	0.81 ± 0.05[c]	
92.2	$(2.9 \pm 0.6) \times 10^{-10}$[d]	$0.6^{+0.2}_{-0.1}$[d]	1.25 ± 0.08
189.5	$(9.0 \pm 0.6) \times 10^{-7}$[d]	0.75 ± 0.02[d]	1.08 ± 0.03
304.0	$(3.08 \pm 0.13) \times 10^{-2}$[e]	0.878 ± 0.010[e]	1.04 ± 0.01

[a]According to the latest adopted level data of ^{26}Al [41].
[b]From Ref. [42].
[c]From Ref. [12].
[d]From Ref. [19].
[e]From Ref. [43].

The direct capture of ^{25}Mg(p, γ)^{26}Al is also calculated based on the present measured spectroscopic factors for the low-lying states and the calculated spectroscopic factors for all the rest bound states in ^{26}Al. Then the derived reaction rates for the ground state, isomeric state, and the total are listed in Table IV, and the total reaction rates and each components are shown in Fig. 6. The contributions of individual resonances have also been calculated via the Monte Carlo method and shown in Fig. 6 as well. The direct capture component can be omitted since the proportion less than 10^{-3} in the total reaction rates at most of the temperature range of astrophysical interest. The 57.7 keV resonance dominates the ^{25}Mg(p, γ)^{26}Al reaction rates at $0.012 \leqslant T_9 \leqslant 0.05$, which
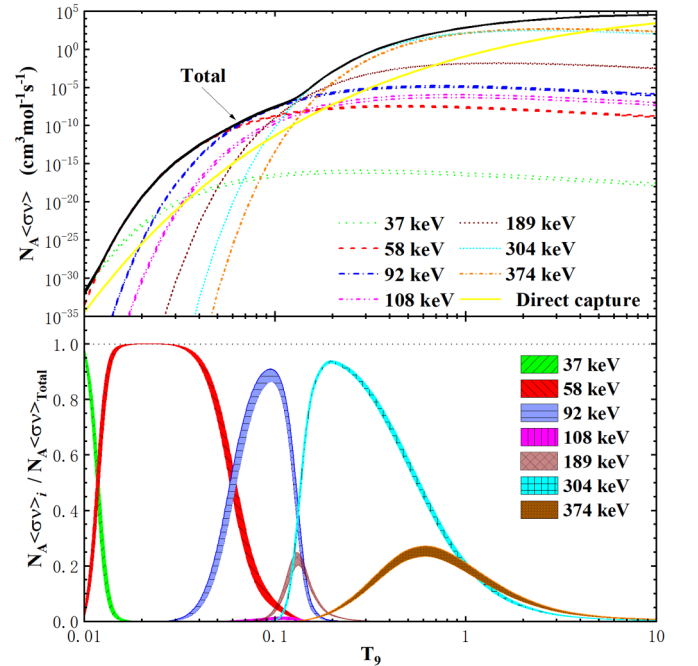

FIG. 6. The present total astrophysical reaction rates and major components of ^{25}Mg(p, γ)^{26}Al in $\pm 1\sigma$ confidence intervals, together with the corresponding proportions of these resonances in the total.

TABLE IV. The present reaction rates for ^{25}Mg$(p,\gamma)^{26}$Al (in $10^{\text{Expt.}}$cm^3 mol^{-1} s^{-1}).

T_9	Total	Ground state	Isomeric state	Expt.
0.010	1.35 ± 0.52	1.06 ± 0.41	0.28 ± 0.13	-32
0.011	7.22 ± 2.28	5.73 ± 1.83	1.48 ± 0.58	-31
0.012	3.42 ± 0.63	2.74 ± 0.52	0.68 ± 0.18	-29
0.013	1.55 ± 0.24	1.25 ± 0.20	0.30 ± 0.08	-27
0.014	5.01 ± 0.82	4.05 ± 0.69	0.95 ± 0.29	-26
0.015	1.07 ± 0.18	0.87 ± 0.15	0.20 ± 0.06	-24
0.016	1.57 ± 0.27	1.27 ± 0.22	0.30 ± 0.09	-23
0.018	1.37 ± 0.23	1.11 ± 0.20	0.26 ± 0.08	-21
0.020	4.82 ± 0.82	3.91 ± 0.69	0.91 ± 0.29	-20
0.025	2.79 ± 0.47	2.26 ± 0.40	0.53 ± 0.17	-17
0.03	1.85 ± 0.31	1.50 ± 0.26	0.35 ± 0.11	-15
0.04	3.29 ± 0.54	2.64 ± 0.46	0.65 ± 0.19	-13
0.05	8.17 ± 1.16	$6.26\,^{+1.01}_{-0.97}$	$1.91\,^{+0.45}_{-0.54}$	-12
0.06	9.20 ± 1.27	$6.48\,^{+1.29}_{-1.01}$	$2.72\,^{+0.68}_{-1.05}$	-11
0.07	6.49 ± 1.06	$4.27\,^{+1.15}_{-0.81}$	$2.22\,^{+0.64}_{-1.03}$	-10
0.08	3.10 ± 0.57	$1.96\,^{+0.62}_{-0.43}$	$1.14\,^{+0.35}_{-0.57}$	-9
0.09	1.08 ± 0.21	$0.67\,^{+0.23}_{-0.16}$	$0.41\,^{+0.13}_{-0.21}$	-8
0.10	3.03 ± 0.58	$1.88\,^{+0.65}_{-0.44}$	$1.15\,^{+0.36}_{-0.59}$	-8
0.11	7.46 ± 1.34	$4.69\,^{+1.48}_{-1.02}$	$2.76\,^{+0.83}_{-1.35}$	-8
0.12	1.83 ± 0.27	$1.22\,^{+0.29}_{-0.20}$	$0.61\,^{+0.16}_{-0.27}$	-7
0.13	5.21 ± 0.48	$3.80\,^{+0.52}_{-0.37}$	$1.41\,^{+0.29}_{-0.47}$	-7
0.14	1.79 ± 0.09	$1.43\,^{+0.10}_{-0.07}$	$0.37\,^{+0.05}_{-0.08}$	-6
0.15	6.62 ± 0.26	$5.52\,^{+0.24}_{-0.22}$	$1.09\,^{+0.09}_{-0.13}$	-6
0.16	2.32 ± 0.09	1.98 ± 0.08	0.34 ± 0.03	-5
0.18	2.08 ± 0.08	1.80 ± 0.08	0.28 ± 0.02	-4
0.20	1.25 ± 0.05	1.08 ± 0.05	0.16 ± 0.01	-3
0.25	3.16 ± 0.13	2.72 ± 0.11	0.43 ± 0.03	-2
0.30	2.73 ± 0.10	2.33 ± 0.09	0.40 ± 0.03	-1
0.35	1.28 ± 0.05	1.08 ± 0.04	0.20 ± 0.01	0
0.40	4.10 ± 0.14	3.43 ± 0.13	0.67 ± 0.04	0
0.45	1.02 ± 0.03	0.85 ± 0.03	0.18 ± 0.01	1
0.50	2.15 ± 0.07	1.77 ± 0.07	0.39 ± 0.02	1
0.60	6.71 ± 0.22	5.40 ± 0.21	1.32 ± 0.07	1
0.70	1.55 ± 0.05	1.22 ± 0.05	0.33 ± 0.02	2
0.80	2.94 ± 0.10	2.28 ± 0.09	0.66 ± 0.04	2
0.90	4.89 ± 0.18	3.73 ± 0.16	1.16 ± 0.07	2
1.00	7.41 ± 0.30	5.57 ± 0.24	1.84 ± 0.11	2
1.25	1.60 ± 0.07	1.17 ± 0.05	0.43 ± 0.03	3
1.50	2.73 ± 0.13	1.95 ± 0.09	0.78 ± 0.05	3
1.75	4.07 ± 0.19	2.86 ± 0.13	1.21 ± 0.07	3
2.0	5.57 ± 0.25	3.86 ± 0.17	1.70 ± 0.09	3
2.5	8.59 ± 0.35	5.81 ± 0.23	2.75 ± 0.13	3
3.0	1.19 ± 0.04	0.80 ± 0.03	0.39 ± 0.02	4
3.5	1.52 ± 0.05	1.02 ± 0.03	0.49 ± 0.02	4
4.0	1.82 ± 0.05	1.22 ± 0.04	0.58 ± 0.02	4
5.0	2.31 ± 0.06	1.55 ± 0.05	0.72 ± 0.02	4
6.0	2.66 ± 0.06	1.79 ± 0.05	0.81 ± 0.03	4
7.0	2.90 ± 0.07	1.93 ± 0.06	0.86 ± 0.03	4
8.0	3.04 ± 0.07	2.01 ± 0.07	0.88 ± 0.03	4
9.0	3.13 ± 0.07	2.04 ± 0.08	0.88 ± 0.03	4
10.0	3.17 ± 0.07	2.04 ± 0.09	0.87 ± 0.03	4

TABLE V. Fitting parameters for the astrophysical reaction rates of the 57.7 keV resonance.

a_0	a_1	a_2	a_3	a_4	a_5	a_6
-16.86	-0.6697	0.006	-0.016	0.0	0.0	-1.495

plays an important role for the massive stars in convective core H-burning region [47]. As the temperature increase at $0.05 \leqslant T_9 \leqslant 0.1$, the proportion of the 57.7 keV resonance decrease from $79.3\% \pm 4.5\%$ to $6.0\% \pm 1.4\%$ in the total reaction rates.

The updated reaction rate of the 57.7 keV resonance have been fitted with the expression used in the REACLIB [48],

$$N_A\langle\sigma v\rangle = \exp\left(a_0 + a_1 T_9^{-1} + a_2 T_9^{-1/3} + a_3 T_9^{1/3} + a_4 T_9 \right.$$
$$\left. + a_5 T_9^{5/3} + a_6 \ln T_9\right). \quad (6)$$

The values of fit parameters $a_{0\sim6}$ are listed in Table V, and the fitting errors are less than 1% in the temperature range of $0.01 < T_9 < 10$.

The present reaction rates are compared with the results of NACRE [44], Iliadis *et al.* [42], and Straniero *et al.* [20] as shown in Fig. 7. The present results keep consistent with the previous data at stellar temperature with $T_9 \geqslant 0.1$, the present center values are about 15% larger than NACRE and about 5% larger than the other two results at key temperature of 57.7 keV resonance and the uncertainty of $\pm 1\sigma$ confidence intervals are much reduced for the total and the ground state. According to the model calculations of convective core H
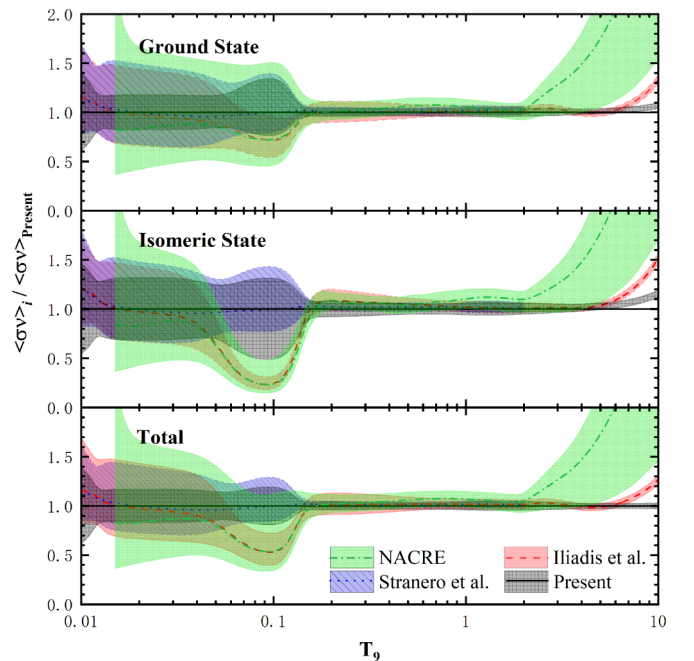

FIG. 7. Comparison between the present recommended reaction rates of ^{25}Mg$(p,\gamma)^{26}$Al and those reported by NACRE [44], Iliadis *et al.* [42] and Straniero *et al.* [20] in dashed and dotted lines, respectively. The grid, dotted, shaded, and slash areas represent the corresponding $\pm 1\sigma$ uncertainties of the present and the other works, respectively.

burning [47], the present enhancement of 57.7 keV resonance impact on the production of ^{26}Al within 20%, and the present smaller uncertainty also can help to understand the contribution of ^{26}Al production in binary star systems [49].

V. SUMMARY

The angular distributions of ^{25}Mg(^{7}Li, ^{6}He)^{26}Al leading to the ground state, first ten, and 6.364 MeV excited states in ^{26}Al have been measured by the Q3D magnetic spectrometer at 31.5 MeV. Based on the shell model calculated proportion of each components in the spectroscopic factors, the proton spectroscopic factors of measured states in ^{26}Al have been derived, then the proton width and resonant strength of 57.7 keV resonance in the ^{25}Mg(p, γ)^{26}Al reaction have been deduced, and following the astrophysical ^{25}Mg(p, γ)^{26}Al reaction rates have been updated. The present results provide independent examinations to the ^{26}Al$^*_{6.364}$ proton spectroscopic factors

and 57.7 keV resonance strength, the ^{25}Mg(p, γ)^{26}Al reaction rates increased about 5% at key temperature of 57.7 keV resonance and the uncertainty are much reduced. This result also lay out a good basement for planned direct measurement of ^{25}Mg(p, γ)^{26}Al reaction in Jinping Underground Laboratory [50].

[1] W. Mahoney, J. Ling, W. Wheaton, and A. Jacobsan, Astrophys. J. **286**, 578 (1984).

[2] S. Plüschke, R. Diehl, V. Schöenfelder, H. Bloemen, W. Hermsen, K. Bennett, C. Winkler, M. McConnell, J. Ryan, U. Oberlack, and J. Knoedlseder, ESA SP **459**, 55 (2001).

[3] R. Diehl, H. Halloin, K. Kretschmer, G. G. Lichti, V. Schönfelder, A. W. Strong, A. V. Kienlin, W. Wei, P. Jean, and J. Knödlseder, Nature (London) **439**, 45 (2006).

[4] C. Gray and W. Compston, Nature (London) **251**, 495 (1974).

[5] P. Hoppe, S. Amari, E. Zinner, T. Ireland, and R. Lewis, Astrophys. J. **430**, 870 (1994).

[6] M. Lugaro, U. Ott, and A. Kereszturi, Prog. Part. Nucl. Phys. **102**, 1 (2018).

[7] R. Betts, H. Fortune, and D. Pullen, Nucl. Phys. A **299**, 412 (1978).

[8] A. Champagne, A. Howard, and P. Parker, Nucl. Phys. A **402**, 159 (1983).

[9] A. Champagne, A. Howard, and P. Parker, Nucl. Phys. A **402**, 179 (1983).

[10] A. Champagne, A. McDonald, T. Wang, A. Howard, P. Magnus, and P. Parker, Nucl. Phys. A **451**, 498 (1986).

[11] P. Endt, P. d. Wit, and C. Alderliesten, Nucl. Phys. A **459**, 61 (1986).

[12] P. Endt and C. Rolfs, Nucl. Phys. A **467**, 261 (1987).

[13] A. Champagne, A. Howard, M. Smith, P. Magnus, and P. Parker, Nucl. Phys. A **505**, 384 (1989).

[14] A. Rollefson, V. Wijekumar, C. Browne, M. Wiescher, H. Hausman, W. Kim, and P. Schmalbrock, Nucl. Phys. A **507**, 413 (1990).

[15] C. Iliadis, T. Schange, C. Rolfs, U. Schröder, and G. Paulus, Nucl. Phys. A **512**, 509 (1990).

[16] C. Iliadis, L. Buchmann, P. M. Endt, H. Herndl, and M. Wiescher, Phys. Rev. C **53**, 475 (1996).

[17] D. Powell, C. Iliadis, A. Champagne, S. Hale, V. Hansper, R. Surman, and K. Veal, Nucl. Phys. A **644**, 263 (1998).

[18] A. Arazi, T. Faestermann, J. O. Fernández Niello, K. Knie, G. Korschinek, M. Poutivtsev, E. Richter, G. Rugel, and A. Wallner, Phys. Rev. C **74**, 025802 (2006).

[19] F. Strieder, B. Limata, A. Formicola, G. Imbriani, M. Junker, D. Bemmerer, A. Best, C. Broggini, A. Caciolli, P. Corvisiero, H. Costantini, A. DiLeva, Z. Elekes, Z. Fülöp, G. Gervino, A. Guglielmetti, C. Gustavino, G. Gyürky, A. Lemut, M. Marta, C. Mazzocchi, R. Menegazzo, P. Prati, V. Roca, C. Rolfs, C. Rossi Alvarez, E. Somorjai, O. Straniero, F. Terrasi, and H. Trautvetter, Phys. Lett. B **707**, 60 (2012).

[20] O. Straniero, G. Imbriani, F. Strieder, D. Bemmerer, C. Broggini, A. Caciolli, P. Corvisiero, H. Costantini, S. Cristallo, A. DiLeva, A. Formicola, Z. Elekes, Z. Fülöp, G. Gervino, A. Guglielmetti, C. Gustavino, G. Gyürky, M. Junker, A. Lemut, and H. Trautvetter, Astrophys. J. **763**, 100 (2013).

[21] L. Lapikás, J. Wesseling, and R. B. Wiringa, Phys. Rev. Lett. **82**, 4404 (1999).

[22] Z. Li, E. Li, B. Guo, X. Bai, Y. Li, S. Yan, Y. Wang, G. Lian, J. Su, B. Wang, S. Zeng, X. Fang, and W. Liu, Eur. Phys. J. A **44**, 1 (2010).

[23] K. Kemper, R. White, L. Charlton, G. Gunn, and G. Moore, Phys. Lett. B **52**, 179 (1974).

[24] Y. J. Li, Z. H. Li, E. T. Li, X. X. Bai, and W. P. Liu, Eur. Phys. J. A **48**, 13 (2012).

[25] Z. Li, Y. Cheng, C. Yan, J. Yang, Q. Zhang, S. Li, K. Zhao, X. Lu, and C. Jiang, Nucl. Instrum. Methods Phys. Res., Sect. A **336**, 150 (1993).

[26] B. Guo, Z. H. Li, M. Lugaro, J. Buntain, D. Y. Pang, Y. J. Li, J. Su, S. Q. Yan, X. X. Bai, Y. S. Chen, Q. W. Fan, S. J. Jin, A. I. Karakas, E. T. Li, Z. C. Li, G. Lian, J. C. Liu, X. Liu, J. R. Shi, N. C. Shu, B. X. Wang, Y. B. Wang, S. Zeng, and W. P. Liu, Astrophys. J. **756**, 193 (2012).

[27] Z. H. Li, Y. J. Li, J. Su, B. Guo, E. T. Li, K. J. Dong, X. X. Bai, Z. C. Li, J. C. Liu, S. Q. Yan, Y. B. Wang, S. Zeng, G. Lian, B. X. Wang, S. J. Jin, X. Liu, W. J. Zhang, W. Z. Huang, Q. W. Fan, L. Gan, Z. D. Wu, and W. P. Liu, Phys. Rev. C **87**, 017601 (2013).

[28] B. Guo, Z. H. Li, Y. J. Li, J. Su, D. Y. Pang, S. Q. Yan, Z. D. Wu, E. T. Li, X. X. Bai, X. C. Du, Q. W. Fan, L. Gan, J. J. He, S. J. Jin, L. Jing, L. Li, Z. C. Li, G. Lian, J. C. Liu, Y. P. Shen, Y. B. Wang, X. Q. Yu, S. Zeng, L. Y. Zhang, W. J. Zhang, and W. P. Liu, Phys. Rev. C **89**, 012801(R) (2014).

[29] J. M. Figueira, J. O. Fernández Niello, D. Abriola, A. Arazi, O. A. Capurro, E. Barbará, G. V. Martí, D. Martínez Heimann, A. E. Negri, A. J. Pacheco, I. Padrón, P. R. S. Gomes, J. Lubian, T. Correa, and B. Paes, Phys. Rev. C **75**, 017602 (2007).

[30] I. J. Thompson, Computer Phys. Rep. **7**, 167 (1988).

[31] L. Gan, Z. Li, H. Sun, D. Pang, B. Guo, Y. Li, J. Su, S. Yan, E. Li, Y. Wang, G. Lian, Z. Han, X. Li, D. Li, T. Ma, C. Pei, Y. Shen, Y. Su, S. Zeng, Y. Zhou, and W. Liu, Sci. China: Phys., Mech. Astron. **60**, 082013 (2017).

[32] Y. Kucuk, I. Boztosun, and T. Topel, Phys. Rev. C **80**, 054602 (2009).

[33] B. A. Brown and W. D. M. Rae, MSU-NSCL Report No. 524 (2007).

[34] W. E. Ormand and B. A. Brown, Nucl. Phys. A **491**, 1 (1989).

[35] M. Igarashi, Computer Program TWOFNR, Surrey University version, 1977.

[36] C. M. Perey and F. G. Perey, At. Data Nucl. Data Tables **17**, 1 (1976).

[37] W. W. Daehnick, J. D. Childs, and Z. Vrcelj, Phys. Rev. C **21**, 2253 (1980).

[38] C. Iliadis, Nucl. Phys. A **618**, 166 (1997).

[39] A. M. Lane, Rev. Mod. Phys. **32**, 519 (1960).

[40] C. Iliadis, R. Longland, A. Champagne, and A. Coc, Nucl. Phys. A **841**, 251 (2010).

[41] www.nndc.bnl.gov/nudat2/getdatasetClassic.jsp?nucleus= 26AL&unc=nds.

[42] C. Iliadis, R. Longland, A. Champagne, A. Coc, and R. Fitzgerald, Nucl. Phys. A **841**, 31 (2010).

[43] B. Limata, F. Strieder, A. Formicola, G. Imbriani, M. Junker, H. W. Becker, D. Bemmerer, A. Best, R. Bonetti, C. Broggini, A. Caciolli, P. Corvisiero, H. Costantini, A. Dileva, Z. Elekes, Z. Fülöp, G. Gervino, A. Guglielmetti, C. Gustavino, A. Gyürky, Gy. Lemut, M. Marta, C. Mazzocchi, P. Menegazzo, R. Prati,

V. Roca, C. Rolfs, C. Rossi Alvarez, C. Salvo, E. Somorjai, O. Straniero, F. Terrasi, and H. P. Trautvetter, Phys. Rev. C **82**, 015801 (2010).

[44] C. Angulo, M. Arnould, M. Rayet, P. Descouvemont, D. Baye, C. Leclercq-Willain, A. Coc, S. Barhoumi, P. Aguer, C. Rolfs *et al.*, Nucl. Phys. A **656**, 3 (1999).

[45] H. Assenbaum, K. Langanke, and C. Rolfs, Z. Phys. A **327**, 461 (1987).

[46] K. Huang, M. Aoyagi, M. Chen, B. Crasemann, and H. Mark, At. Data Nucl. Data Tables **18**, 243 (1976).

[47] C. Iliadis, A. Champagne, A. Chieffi, and M. Limongi, Astrophys. J. Suppl. **193**, 16 (2011).

[48] T. Thielemann, M. Arnould, and J. Truran, in *Advances in Nuclear Astrophysics*, edited by E. Vangioni-Flam, J. Audouze, M. Cassé *et al.*, (Editons Frontiers, Gif-sur-Yvette, 1987).

[49] H. Brinkman, C. Doherty, O. Pols, E. Li, B. Côté, and M. Lugaro, Astrophys. J. **884**, 38 (2019).

[50] W. Liu, Z. Li, J. He, X. Tang, G. Lian, Z. An, J. Chang, H. Chen, Q. Chen, X. Chen, Z. Chen, B. Cui, X. Du, C. Fu, L. Gan, B. Guo, G. He, A. Heger, S. Hou, H. Huang, N. Huang, B. Jia, L. Jiang, S. Kubono, J. Li, K. Li, T. Li, Y. Li, M. Lugaro, X. Luo, H. Ma, S. Ma, D. Mei, Y. Qian, J. Qin, J. Ren, Y. Shen, J. Su, L. Sun, W. Tan, I. Tanihata, S. Wang, P. Wang, Y. Wang, Q. Wu, S. Xu, S. Yan, L. Yang, Y. Yang, X. Yu, Q. Yue, S. Zeng, H. Zhang, H. Zhang, L. Zhang, N. Zhang, Q. Zhang, T. Zhang, X. Zhang, X. Zhang, Z. Zhang, W. Zhao, Z. Zhao, and C. Zhou, Sci. China: Phys., Mech. Astron. **59**, 642001 (2016).

Correction: Reference [30] contained the wrong author and source listing and has been fixed.

Second Correction: New References [30] and [34] were added and subsequent references have been renumbered.